Cytokine 173 (2024) 156419

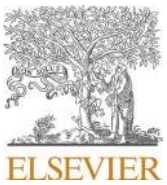

Contents lists available at ScienceDirect

Cytokine

journal homepage: www.elsevier.com/locate/cytokine

The role of macrophage polarization and related key molecules in pulmonary inflammation and fibrosis induced by coal dust dynamic inhalation exposure in Sprague-Dawley rats

Rui Wang [a,b], Siyi Zhang [c], Yifei Liu [a,b], Hongmei Li [d], Suzhen Guan [a,b], Lingqin Zhu [a,b], Leina Jia [a,b], Zhihong Liu [a,b,*], Haiming Xu [a,b,*]

[a] School of Public Health, Ningxia Medical University, Yinchuan, Ningxia 750004, China
[b] The Key Laboratory of Environmental Factors and Chronic Disease Control of Ningxia, No. 1160, Shengli Street, Xingqing District, Yinchuan, Ningxia 750004, China
[c] Wuxi Center For Disease Control And Prevention, Wuxi, Jiangsu 214000, China
[d] The Key Laboratory of Fertility Preservation and Maintenance of Ministry of Education, Ningxia Medical University, Yinchuan, Ningxia 750004, China

ARTICLE INFO

Keywords:
Coal dust
Pulmonary inflammation and fibrosis
Macrophage polarization
Dynamic inhalation exposure
Cytokine

ABSTRACT

Coal dust is the main occupational hazard factor during coal mining operations. This study aimed to investigate the role of macrophage polarization and its molecular regulatory network in lung inflammation and fibrosis in Sprague-Dawley rats caused by coal dust exposure. Based on the key exposure parameters (exposure route, dose and duration) of the real working environment of coal miners, the dynamic inhalation exposure method was employed, and a control group and three coal dust groups (4, 10 and 25 mg/m^3) were set up. Lung function was measured after 30, 60 and 90 days of coal dust exposure. Meanwhile, the serum, lung tissue and bronchoalveolar lavage fluid were collected after anesthesia for downstream experiments (histopathological analysis, RT-qPCR, ELISA, etc.). The results showed that coal dust exposure caused stunted growth, increased lung organ coefficient and decreased lung function in rats. The expression level of the M1 macrophage marker iNOS was significantly upregulated in the early stage of exposure and was accompanied by higher expression of the inflammatory cytokines TNF-α, IL-1β, IL-6 and the chemokines IL-8, CCL2 and CCL5, with the most significant trend of *CCL5* mRNA in lung tissues. Expression of the M2 macrophage marker Arg1 was significantly upregulated in the mid to late stages of coal dust exposure and was accompanied by higher expression of the anti-inflammatory cytokines IL-10 and TGF-β. In conclusion, macrophage polarization and its molecular regulatory network (especially CCL5) play an important role in lung inflammation and fibrosis in SD rats exposed to coal dust by dynamic inhalation.

1. Introduction

Coal workers' pneumoconiosis (CWP), also known as black lung disease, is a chronic occupational disease caused by the long-term inhalation of coal dust which happens in coal miners. Long-term exposure to coal dust could cause inflammatory and irreversible pulmonary fibrosis [1]. Due to the deficiency of effective medicine and treatment, CWP puts great economic, psychological, and physical burdens on patients, as well as incalculable economic loss to society [2]. The etiology of CWP has been clearly established, but the specific pathogenesis remains the focus of current research into occupational diseases.

Various hypotheses have been proposed for the pathogenesis of pneumoconiosis, including mechanical stimulation, chemical toxicity, autoimmunity, oxidative stress, cytokine networks, etc. However, none of them can fully describe the pathogenesis of pneumoconiosis. It is generally considered that dust stimulates macrophages to induce persistent inflammation and tissue injury leading to a cycle of aberrant repair which promotes fibrosis [3]. Pulmonary macrophages are the most numerous immune cells present in the lung, alveolar space and alveolar cavity which have strong abilities to recognize and kill pathogens, as well as to take up, process and present antigens, playing a key role in resolving inflammation, defending against exogenous pathogens and maintaining lung homeostasis [4–5]. When dust enters lung tissue as a non-specific antigen, it is firstly phagocytosed by macrophages,

* Corresponding authors at: School of Public Health, Ningxia Medical University, Yinchuan, Ningxia 750004, China.
E-mail addresses: zhihongliu2021@163.com (Z. Liu), xuhaiming5689467@163.com (H. Xu).

https://doi.org/10.1016/j.cyto.2023.156419
Received 5 September 2023; Received in revised form 26 October 2023; Accepted 1 November 2023

which are stimulated to secrete various inflammatory factors and chemokines to initiate a strong inflammatory response that can damage lung tissue [6–7]. When the dust-containing macrophages die, the released dust will be re-engulfed by other macrophages, a process that repeats itself and leads to a cycle of inflammatory damage [8]. Over time, the acute inflammatory response in the lungs gradually subsides into chronic inflammation, accompanied by the onset of tissue repair. Macrophages can initiate fibrosis by secreting fibrosis-associated factors that activate fibroblasts in lung tissue to differentiate into myofibroblasts, which are important effector cells for tissue repair that secrete collagen 1 (Col-1) and fibronectin (FN1) to promote tissue repair [9–10]. Thus, macrophages become the key cells in the pathogenesis of pneumoconiosis.

The process by which macrophages have been activated at an indicated point in space and time is here referred to as macrophage polarization [11]. Previous research showed that macrophage polarization is critical to the initiation and resolution of lung inflammation and fibrosis [5,12]. In general, macrophage polarization can be divided into classically activated (M1) and alternatively activated (M2) types [13]. M1 macrophages, also known as pro-inflammatory macrophages, are induced mainly by lipopolysaccharide (LPS) and interferon-gamma (IFN-γ) with inducible nitric oxide synthase (iNOS) as their specific markers. M1 macrophages secrete pro-inflammatory factors (IL-6, IL-1β, TNF-α, etc.) and chemokines (CCL2, CCL5, IL-8, etc.), exerting pro-inflammatory and cytotoxic effects. Conversely, M2 macrophages, also known as anti-inflammatory macrophages, are activated by interleukin 4 (IL-4) and interleukin 13 (IL-13), specifically expressing arginase 1 (Arg1), etc. M2 macrophages also secrete anti-inflammatory and pro-fibrotic factors (IL-10, TGF-β, etc.) and are involved in the suppression of inflammation, tissue remodeling, and immune regulation [14–19]. When an injury occurs, M1 macrophages and M2 macrophages have a clear division of function. M1 macrophage polarization always occurs in the early stages of injury and is associated with pro-inflammatory responses, bacterial clearance, and tumoricidal activity, while M2 macrophages play an important role in coordinating inflammatory elimination and immunosuppression [5]. Self-limiting properties of macrophage polarization are essential for the elimination of exogenous substances [11]. According to research, altering macrophage polarization could reduce the symptoms of pulmonary fibrosis [20–21], suggesting that macrophage polarization may play an important role in the development and progression of CWP.

Most of the current studies have investigated the relationship between macrophage polarization and silicosis by constructing models through single endotracheal instillation, while relatively few studies have investigated macrophage polarization and CWP [10,20]. The methods described above do not simulate actual working exposure patterns and may cause respiratory inflammation due to improper handling, which may interfere with the subsequent determination of inflammatory parameters. Therefore, this study aimed to investigate the association between macrophage polarization and CWP by observing the dynamic changes of macrophage polarization in lung tissue over time in a rat model of CWP constructed by dynamic inhalation exposure, meanwhile, to understand the occurrence of inflammatory and fibrotic markers, as well as the dynamics of these markers over time in different samples, and to provide scientific reference for basic research and treatment strategies for CWP.

2. Materials and methods

2.1. Coal dust and characterization

This study collected deposited dust from a coal mine in Ningxia, China. The collected coal dust was dried in an oven at 120 °C for 4 h for later use [20]. The pyrophosphate method was used for the determination of free silica in coal dust [22]. The infrared spectroscopy was used to analyze the silica-oxygen bonds and characteristic diffraction peaks of coal dust (IRArinity-1, Shimadzu, Japan) [23]. The transmission electron microscope (H-7560, Hitachi, Japan) and the scanning electron microscope (S-3400 N, Hitachi, Japan) were employed to observe the size and morphology of coal dust particles [24]. The nanoparticle sizer was used to determine the particle size and stability of coal dust (ZEN3690, Malvern, UK) [25].

2.2. Animal and dynamic inhalation exposure

Male Sprague-Dawley (SD) rats were provided from the Experimental Animal Centre of Ningxia Medical University, 6–8 weeks old, total number of 80, with weight difference < 20% compared to average weight. The experimental procedures were reviewed by the Experimental Animal Ethics Committee of the Laboratory Animal Center of Ningxia Medical University (No.2021-N0093).

The rats were bred in an animal house with a temperature of 22 °C ± 3 °C, a relative humidity between 30% and 70%, a light/dark cycle of 12 h, a standard diet and free access to water. The animals were weighed and numbered priorly to the test and grouped using a completely randomized grouping method.

There was one control group and three coal dust groups in this study. According to the < Occupational exposure limits for hazardous agents in the workplace - Part 1: Chemical hazardous agents > formulated by the National Health Commission, the permissible concentration - time weighted average (PC-TWA) of total coal dust (free SiO_2 content < 10%) is 4 mg/m^3, and special provisions are made for exceeding the limit value by a factor of 3 times and 5 times. Therefore, a multiple of 2.5 times was chosen to set three coal dust groups, namely low (4 mg/m^3), medium (10 mg/m^3) and high (25 mg/m^3), with 20 rats in each group. The experiments were conducted using a dynamic inhalation exposure instrument (HOPE-MED8050, Tianjin, China) for exposure (Ventilation Volume per hour: 12–15 times, oxygen contents: 21%, weak negative pressure, airflow rate: 0.3–0.8 m^3/h, temperature: 22 °C ± 2 °C, relative humidity: 40% − 70%). The total volume of animals should not exceed 5% of the total volume of the cabinet in order to adequately expose the animals to the test sample. The experiment was conducted for a total of 90 days, with 6 days of exposure each week and 4 h of exposure for each group a day. The weight of each rat was recorded at 10 - day intervals. After 30, 60 and 90 days of coal dust exposure, six rats in each group were randomly selected for pulmonary function measurements (Buxco PFT, USA). The rats were anesthetized by inhalation of isoflurane and apical blood sampling was performed. After the rats had been sacrificed, lung tissue and alveolar lavage fluid was taken for subsequent experiments (Fig. 1).

2.3. Serum, lung tissue and bronchoalveolar alveolar lavage fluid (BALF) collection

Whole blood was collected using a non-anticoagulant blood collection tube, clotted naturally for 30 mins, centrifuged at 4 °C and 2000 g for 15 mins, the upper yellow serum layer was removed and stored at -80 °C.

The lung tissue and tracheobronchial were removed intact, blood and hair were rinsed from the tissue with saline, surface water was aspirated and then weighed and recorded, which was used to calculate the pulmonary organ coefficient. The upper end of the trachea was clamped with a hemostat, sterile 0.9% physiological saline was withdrawn using a 5 mL syringe, and slowly injected into the lung from the trachea at the lower side of the hemostat. Then, the lung was gently pressed and left for 30 s to extract the lavage fluid, which was repeated 3 times with a recovery rate of approximately 80%. After collection, the supernatant was centrifuged at 3000 g for 10 mins at 4 °C and stored in aliquots at -80 °C for subsequent experiments.

After perfusion, the first lobe of right lung was cut off and weighed (W) and then placed in an -80 °C incubator to dry to a constant weight (D), which was used to calculate the wet-to-dry weight ratio (W/D) of

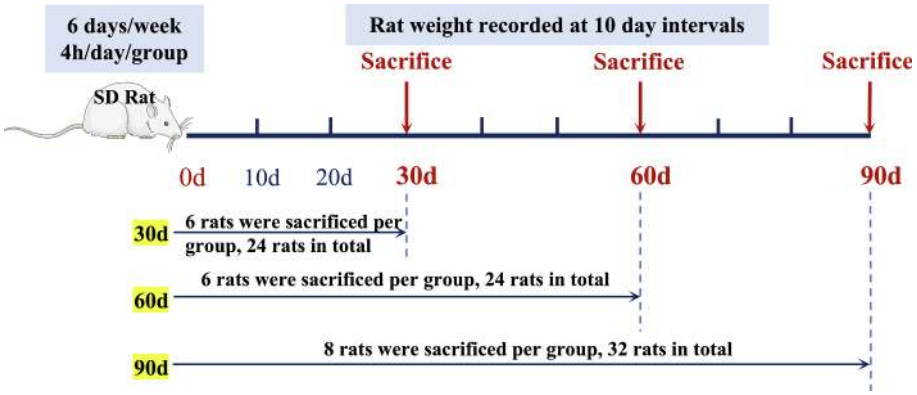

Fig. 1. Schematic diagram of a dynamic inhalation exposure experiment.

the lung tissue. The fourth lobe of the right lung was fixed and preserved in a 4% paraformaldehyde fixative. The remaining lung tissue was frozen at -80 °C in a freezer for subsequent total RNA extraction.

2.4. Histology

Completely fixed lung tissue was embedded in paraffin, which was cut into sections of 4–6 μm thickness for hematoxylin and eosin staining (HE staining) to observe inflammatory changes in the lung tissue. The sections were scored for the inflammatory response on the basis of referring to the quantitative analysis standards proposed in Szapiel and Elson's research [26]. Masson's trichrome staining was used to visualize fibrosis in the lung tissue. The percentage of positive expression area (Area%) was calculated using ImageJ software (National Institutes of Health, USA) for statistical analysis. Sections were incubated with rabbit anti-mouse primary antibodies against CD68 (1:100) (Abcam, UK), iNOS (1:2000) (Abcam, UK), and Arg1 (1:750) (Wuhan Servicebio Technology Co., Ltd., China), followed by horseradish peroxidase (HRP) - coupled goat anti-rabbit IgG secondary antibody (Zhongshan Jinqiao Biotechnology Co., Ltd., China), and average optical density (AOD) were calculated by ImageJ software for statistical analysis.

2.5. Quantitative real-time polymerase chain reaction (qRT-PCR)

The rat lung tissue was taken out from -80 °C and placed in a centrifuge tube prefilled with RNA lysate for homogenization operation (4 °C), fully ground and centrifuged (13400 g, 4 °C, 10 mins), and the supernatant was extracted. Total RNA extraction, reverse transcription, and qRT-PCR operation were performed in strict accordance with the kit instructions (Tiangen Biochemical Technology (Beijing) Co., Ltd., China). Using β-actin as the internal reference gene, three replicate wells were set up for each sample, and the relative expression of the gene was calculated using the $2^{-\Delta\Delta Ct}$ method. All primers (synthesized by Bioengineering (Shanghai) Co., Ltd., China) were verified for specificity by Primer-BLAST (https://blast.ncbi.nlm.nih.gov), and the primer sequences are shown in Table 1.

2.6. Enzyme-linked immunosorbent assay, ELISA

Soluble cytokines including IL-1β, IL-6, TNF-α, MCP-1, CCL5, IL-8, TGF-β, IL-10, Gas6 in rat serum, lung tissue, and BALF were determined using commercially available ELISA assay kits according to the instructions. All experimental steps were operated in strict accordance with the kit instructions.

2.7. Statistics

SPSS 24.0 statistical software (SPSS Inc, Chicago, USA) was applied for data processing and analysis, and GraphPad Prism 9 (GraphPad Software LLC, Boston, USA) was used for graphing. All data are expressed as mean ± SD. Means between two groups of samples were compared using *t*-test, and means between multiple groups of samples were compared using one-way ANOVA, with differences considered significant at $P < 0.05$.

Table 1
qRT-PCR primer sequences.

Gene Name	Genbank Accession No.	Forward primer(5′-3′)	Reverse primer(5′-3′)	Product length
β-actin	NM_031144.3	CCAGATCATGTTTGAGACCTTCAA	GTGGTACGACCAGAGGCATACA	87
TNF-α	NM_012675.3	GTGATCGGTCCCAACAAG	AGGGTCTGGGCCATGGAA	71
IL-6	NM_012589.2	CCGGAGAGGAGACTTCACAGAGGA	AGCCTCCGACTTGTGAAGTGGTATA	71
IL-1β	NM_031512.2	CGTCCTCTGTGACTCGTGG	TCGTTGCTTGTCTCTCCTT	138
CCL2	NM_031530.1	CTGTAGCATCCACGTGCTGT	AGTTCTCCAGCCGACTCATTG	104
CCL5	NM_031116.3	ACCACTCCCTGCTGCTTTG	ACACTTGGCGGTTCCTTCG	130
IL-8	NM_030845.2	CCCCCATGGTTCAGAAGATTG	TTGTCAGAAGCCAGCGTTCAC	113
IL-10	NM_012854.2	CATCCGGGGTGACAATAA	TGTCCAGCTGGTCCTTCT	119
Gas6	NM_057100.2	CCCCCGTGATTAGACTACGC	GATCCAGGTGCTATCCGAGC	128
TGF-β	NM_021578.2	GACTCTCCACCTGCAAGACCAT	GGGACTGGCGAGCCTTAGTT	101
FN1	NM_019143.2	GTGGCTGCCTTCAACTTCTC	GTGGGTTGCAAACCTTCAAT	132
Col-1	NM_053304.1	ACTGGTACATCAGCCCAAAC	GGAACCTTCGCTTCCATACTC	98
E-cad	NM_031334.1	GAGGTCTTTGAGGGATCTGTTG	GGCAGCATTGTAGGTGTTTATG	105
α-SMA	NM_031004.2	AGGGAGTGATGGTTGGAATG	GGTGATGATGCCGTGTTCTA	110
CD68	NM_001031638.1	CGCCAGTGACCAATCTCTC	GGGTAACGCAGAAGGCAAT	92
iNOS	NM_012611.3	AGACGCACAGGCAGAGGT	AGGCACACGCAATGATGG	119
Arg1	NM_017134.3	TTGGAACGAAACGGGAAGGT	TGTTCGGTTTGCTGTGATGC	113

3. Results

3.1. Characterization of coal dust

3.1.1. Determination of free silica (SiO_2) content in coal dust

The pyrophosphoric acid method was used to determine the free SiO_2 content in coal dust at 3.855%. As stipulated, coal dust containing less than 5% free silica is called pure coal dust, so the coal dust used in this experiment was pure coal dust.

3.1.2. Analysis of the infrared spectroscopy results

There were five distinct absorption peaks in the coal dust, as shown in Fig. 2A. The most obvious one was the absorption peak in the 1020–1060 cm^{-1} band, which indicated the asymmetrical stretching vibration of Si—O—Si. The absorption peak at around 470 cm^{-1} may indicate a symmetrical stretching vibration of Si—O, the large sharp peak appearing at around 540 cm^{-1} indicates a rotational isomeric absorption band of C—Br, and the peak at around 1610 cm^{-1} indicated an aromatic C=C skeleton stretching vibration. There was a broadened absorption peak near 3400 cm^{-1}, belonging to OH groups and water in coal [27]. In addition, the absorption peaks in the 600–730 cm^{-1} band indicated C—S stretching vibrations, but the absorption peaks were inconspicuous, which was similar to the results obtained for the infrared spectra.

3.1.3. Analysis of transmission electron microscopy and scanning electron microscopy results

Fig. 2B showed the results of transmission electron microscopy and scanning electron microscopy. The transmission electron microscopy image (Fig. 2B a-b) showed the irregular shape of the coal dust with a lamellar structure and the presence of agglomeration. According to the scanning electron microscopy image (Fig. 2B c-d), the shape and size of the coal dust varied, with particle sizes ranging from approximately 10–100 μm, again in a lamellar-like structure, in accordant with the transmission electron microscopy results.

3.1.4. Nanoparticle size measurement of the hydrated particle size and zeta potential of coal dust

Zeta potential is also known as electromotive force. Its value reflects the stability of the substance in the dispersion system. The higher the value of the zeta potential, the more stable the system. On the contrary, it indicates that the detected substance is in an unstable state in the dispersion system. A zeta potential of around ± 30 mV is generally considered not to quickly settle and would be suspended and distributed in the dispersion systems [28]. The results of nanoparticle size measurement indicated that coal dust in water had a particle size of approximately 2000–2500 nm in water and does not quickly settle and would be suspended (Table 2).

Table 2
Hydrated particle size and zeta potential of coal dust in dispersion systems.

Dispersion system	Hydrated particle size (nm)	Zeta potential (mV)
5 μg/ml ddH_2O	2450	−16.1
10 μg/ml ddH_2O	2383	−18.3
50 μg/ml ddH_2O	2354	−22.2

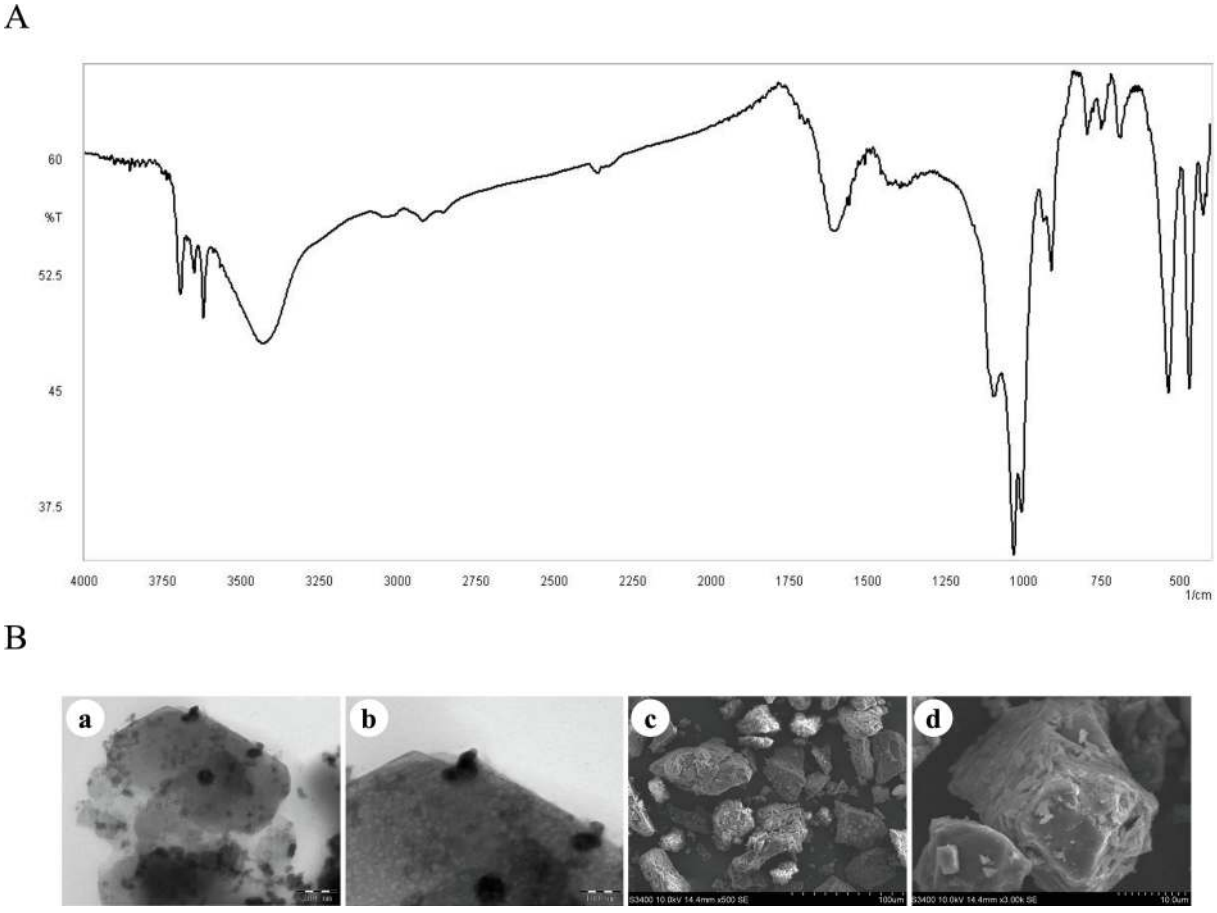

Fig. 2. Results of the coal dust characterization. A shows the infrared spectra analyzed for coal dust. B shows the analysis of coal dust transmission electron microscopy and scanning electron microscopy results. a-b show the results of transmission electron microscopy, magnifications of a and b are 15000 and 30000 times respectively. c-d shows the results of scanning electron microscopy, magnifications of c and d are 500 and 3000 times respectively.

3.2. Changes in general indicators in rats caused by coal dust exposure

3.2.1. Weight change

Compared with the weight at the starting point of the experiment, the control group increased 1.64 times more weight at the end of the experiment, and gained 1.16, 1.27 and 1.17 times more weight in the low, medium and high groups respectively. This indicated that the trend of weight gain in the coal dust group was slower as the duration of coal dust exposure increased compared with the control group (Fig. 3A). As shown in Fig. 3B, after 30 days of coal dust exposure, the body weight of rats in all coal dust exposure groups tended to increase compared with the control group, and the difference was statistically significant ($P < 0.01$). At 60 days of coal dust exposure, the body weights of rats in all coal dust exposure groups were reduced compared with the control group, but only the difference between the high-dose group and the control group was statistically significant ($P < 0.05$). At 90 days of coal dust exposure, rats in all coal dust exposure groups showed a trend of decreasing body weight compared with the control group, with a statistically significant difference ($P < 0.05$). The results indicated that coal dust caused a slower increase in body weight in rats as the dose and duration of coal dust exposure increased.

3.2.2. Changes in organ coefficients and wet/dry weight ratios of rat lung tissue

As shown in Fig. 3C, there were no statistical differences in the lung organ coefficients between the groups at 30 and 60 days of coal dust exposure ($P > 0.05$). After 90 days of coal dust exposure, the lung organ coefficients were significantly higher in all coal dust exposure groups compared with control group (all $P < 0.05$). According to Fig. 3D, at 30, 60 and 90 days of coal dust exposure, there was no significant change in the lung wet/dry weight ratio in the low, medium and high dose groups compared with the control group at the corresponding time point ($P > 0.05$).

3.3. Changes in lung function indicators

As shown in Table 3, lung function of the rats could be affected by coal dust exposure. After 30 days of coal dust exposure, the respiratory rate, tidal volume, vital capacity and inspiratory capacity of rats in the dose groups showed an increase compared with the control group, and

Table 3
SD rat lung function index (Mean±SD).

Group		Tidal volume (mL)	Respiratory rate (times/min)	Vital capacity (mL)	Inspiratory capacity (mL)
30d	C	59.83 ± 0.31	5.75 ± 0.25	31.44 ± 1.47	26.86 ± 1.89
	L	60.07 ± 0.03	5.98 ± 0.28	33.64 ± 2.18	28.81 ± 2.61
	M	60.05 ± 0.07	6.01 ± 0.06*	33.94 ± 2.12	29.21 ± 1.58
	H	60.13 ± 0.18	6.11 ± 0.16*	38.27 ± 4.70*	32.38 ± 3.36*
60d	C	59.95 ± 0.03	5.29 ± 0.17	28.80 ± 0.63	24.72 ± 1.05
	L	59.90 ± 0.14	4.65 ± 0.86	29.14 ± 2.12	24.91 ± 1.87
	M	60.82 ± 0.59	4.59 ± 0.22*	26.19 ± 2.81*	24.92 ± 0.80
	H	61.27 ± 0.58*	4.36 ± 0.06#	24.94 ± 2.21#	23.60 ± 0.28
90d	C	59.83 ± 1.00	5.76 ± 0.25	27.19 ± 1.47	26.02 ± 0.68
	L	60.40 ± 0.32	5.70 ± 0.03	25.72 ± 0.98*	25.67 ± 0.74*
	M	60.64 ± 0.73*	4.98 ± 0.54	25.58 ± 1.16*	24.78 ± 0.61#
	H	62.16 ± 0.77#	3.93 ± 0.52#	23.84 ± 0.60#	23.98 ± 0.61#

Note: C, control group; L, low-dose coal dust group; M, medium-dose coal dust group; H, high-dose coal dust group. $n = 6$. Compared with the control group at the corresponding time points, *$P < 0.05$, #$P < 0.01$.

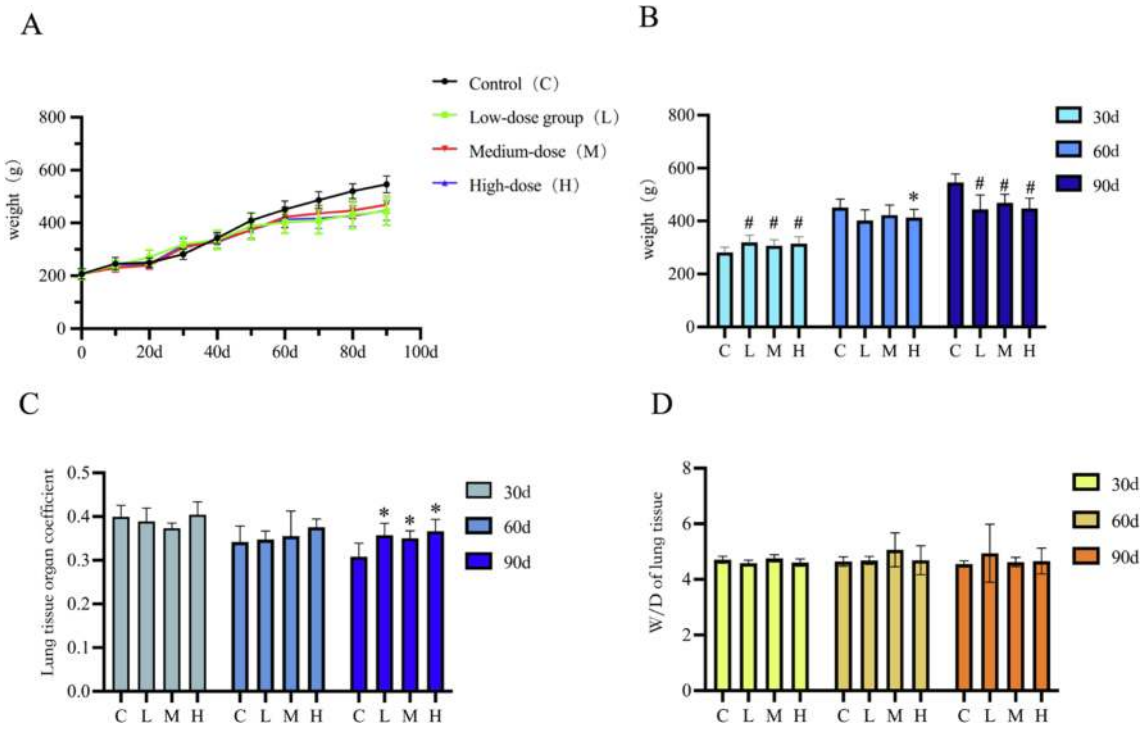

Fig. 3. A is a line graph of the body weight of rats, B is a histogram of rat body weight, C is the lung tissue organ factor, D is the wet/dry weight ratio of the lung tissue. $n = 6$. Compared with the control group at the corresponding time points, *$P < 0.05$, #$P < 0.01$.

the difference in respiratory rate was not statistically significant ($P > 0.05$), the difference in tidal volume between the medium and high dose groups was statistically significant ($P < 0.05$). The difference in vital capacity and inspiratory capacity was statistically significant ($P < 0.05$) only in the high dose group, with increases of 21.72% and 20.55%, respectively. After 60 and 90 days of coal dust exposure, the respiratory rate was significantly higher ($P < 0.05$) and tidal volume, vital capacity, and inspiratory capacity were significantly lower (all $P < 0.05$) compared with the control group. The above results indicated that coal dust induced ventilatory limitation and reduced lung function of the rats.

3.4. Effect of coal dust exposure on histopathological changes in rat lung

3.4.1. Histomorphological observation

From Fig. 4A-C (a-d), it can be observed that the lung tissues of the control groups were rosy in color, exhibited a plump morphology and rebounded quickly after finger pressure, whereas the lung tissues of the coal dust group were Not plump in morphology, darker in color, less elastic and had petechiae. The lung tissues of the high dose group at 60 and 90 days of coal dust exposure were clearly seen to be shrunken and harden, which was worsens with the increase of exposure time and dose.

3.4.2. HE staining observation of inflammatory changes

As shown in Fig. 4A-C (e-h), the control group had a clear and intact lung tissue structure, no widening of the alveolar septa, normal alveolar wall structure, plump alveoli, and no cellular infiltrates or exudates in the alveolar cavity and no obvious bleeding, edema or inflammatory response were observed. After 30 days of coal dust exposure, a small number of inflammatory cell aggregates, slight thickening of the alveolar wall and slight changes in alveolar structure were observed in the high dose group. The lung tissue inflammatory response score of lung tissue was significantly higher in the high dose group compared with the control group ($P < 0.01$). After 60 days of coal dust exposure, partial alveolar walls begin to break down, a large amount of alveoli fuse or collapse, alveolar septa widen and infiltration of a certain number of inflammatory cells could be observed. After 90 days of coal dust exposure, a large area of lung tissue was damaged, the alveolar lumen was reduced or even atretic, a large number of inflammatory cells were infiltrated, and the lung tissue inflammatory response scores were significantly higher in the medium and high dose groups compared with the control group ($P < 0.01$). These results suggested that the inflammatory response of the lung tissue becomes more intense with increasing duration and dose of coal dust exposure.

3.4.3. Masson staining observation of fibrosis changes

Masson staining can stain the collagen fibers blue-purple. In this study, no significant blue purple collagen fibers were observed in the lung tissue of rats in the control group, and the alveoli were plump and structurally intact. After 30 days of coal dust exposure, collagen fibers deposition in lung tissue was not significant in all coal dust exposure groups compared with the control group ($P > 0.05$). Fig. 4B (i-l) showed that at 60 days of coal dust exposure, there was no significant deposition of collagen fibers in the low dose group compared with the control group, while in the medium and high dose groups significant blue collagen fibers appeared, the alveolar wall began to extrude the alveolar lumen and fibrotic changes appeared in the lung tissue, with a statistically significant difference in the area of positive expression ($P < 0.01$). At 90 days of coal dust exposure, fibrotic changes increased in all coal dust exposure groups compared with the control group, with severe destruction of alveolar structures, band-shaped interstitial collagen fiber hyperplasia, and large area deposition of collagen fibers, with the most severe degree of pulmonary fibrosis in the high dose group (Fig. 4C i-l). Meanwhile, the mRNA expression levels of the epithelial cell marker *E-cad* decreased with increasing duration and dose of coal dust exposure, while the mRNA expression of the mesenchymal cell marker *α-SMA* and the fibrosis markers *Col-1* and *FN1* increased significantly ($P < 0.01$) (Fig. 4D-G).

3.5. Effect of coal dust exposure on macrophage markers CD68, iNOS and Arg1 in rat lung tissue

3.5.1. The protein expression levels of CD68, iNOS and Arg1 in lung tissue

To investigate whether coal dust could affect lung macrophage polarization, the protein expression levels of CD68, iNOS and Arg1 in lung tissue was examined by immunohistochemistry. Brown color indicates positive expression. From Fig. 5A and D, it could be seen that after 30 days of coal dust exposure, the lung tissues of the control, low and medium dose groups were basically free of positive staining areas, whereas scattered areas of positive CD68 expression began to appear in the high dose group, with statistically significant differences in AOD values ($P < 0.05$). After 60 days of exposure, there were no obvious positive areas in the control and low dose groups, scattered brown areas appeared in the medium dose group, and the high dose group showed increased areas of positive expression compared with the 30 days-high dose group. The difference in AOD was more pronounced in the high dose group compared with the control group at 90 days ($P < 0.01$). The above results suggested that increasing the dose and duration of dust exposure leads to an accumulation of macrophages in the lung tissue.

As shown in Fig. 5B and E, the expression of iNOS showed an overall increasing trend with increasing exposure time. The positive expression of iNOS increased with increasing dose after 30 and 60 days of coal dust exposure, with statistically significant differences in AOD in the high dose group compared with the control group at the same time points (all $P < 0.05$). After 90 days of coal dust exposure, the AOD of iNOS was statistically different between the medium, high dose groups and the control group. However, there was a trend towards lower AOD levels in the 90-day high-dose group compared with the 30-day high-dose group.

As with iNOS, Arg1 expression also tended to rise with increasing exposure time (Fig. 5C, F). Unusually, even though the differences in positive expression between each dose group and the control group were not statistically significant ($P > 0.05$), scattered Arg1 positive expression signal began to appear in the high dose group after 30 days of coal dust exposure. After 60 and 90 days of coal dust exposure, sporadic positive expression signal began to appear in the low dose group, while in the medium dose group there were areas of patchy positive reactions, and in the high dose group the areas of positive expression increased even more significantly, with the longer the coal dust exposure, the more significant the positive expression ($P < 0.01$).

3.5.2. The mRNA expression levels of CD68, iNOS and Arg1

The results showed that the mRNA expression level of the macrophage marker *CD68* in rat lung tissues increased with increasing coal dust exposure time and dose, indicating that coal dust may cause macrophage aggregation in rat lung tissues (Fig. 5G).

The mRNA expression levels of the M1 macrophage marker *iNOS* increased with increasing doses of coal dust after 30 and 60 days exposure. Compared with the control group at the same time point, the high dose group showed a significant increase (5.13-fold and 3.78-fold, respectively) ($P < 0.01$). In contrast, there was no significant difference between the coal dust exposure groups and the control group at 90 days (Fig. 5H).

As shown in Fig. 5I, the mRNA expression level of the M2 macrophage marker *Arg1* only showed a non-significant decrease ($P > 0.05$) in the coal dust exposure groups compared with the control group at 30 days. In contrast, at 60 and 90 days of coal dust exposure, there was a trend of increased mRNA expression levels of *Arg1* in each dose group compared to the corresponding control group, and the differences between the high dose group and the respective control groups at the above two time points were statistically significant (2.07-fold and 2.62-fold increase, respectively) ($P < 0.05$).

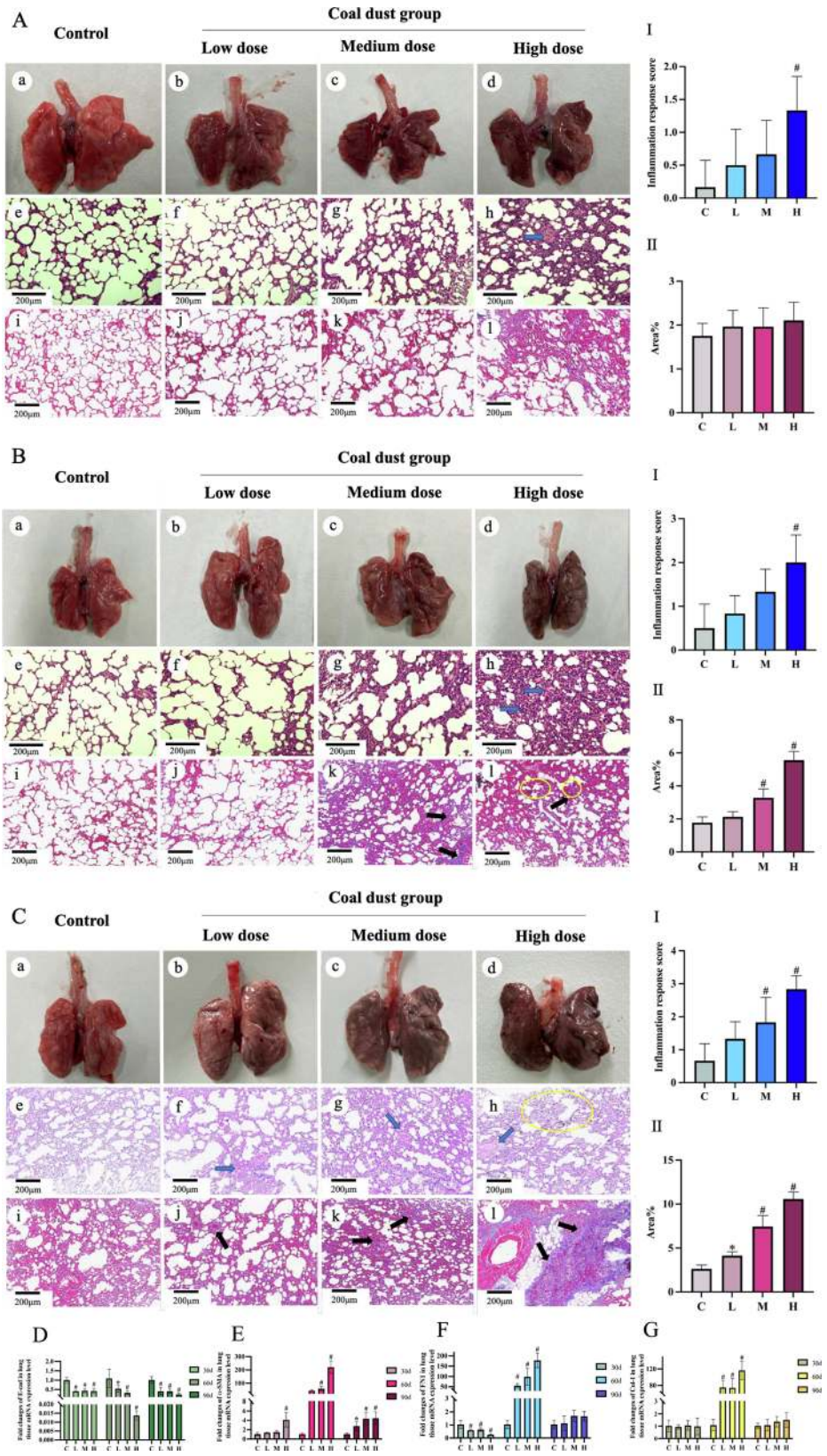

Fig. 4. Map of lung histomorphology and changes in inflammatory lesions and fibrosis in rats. A-C are the results of coal dust exposure experiments for 30, 60 and 90 days respectively; a-d are dissections of rat lung tissue; e-h are HE staining of rat lung tissue (10X); i-l are Masson staining of rat lung tissue (10X); I is the lung tissue inflammatory response score; II for lung tissue fibrosis score. Blue arrows point to areas of inflammatory lesions; red arrows point to areas of fibrous hyperplasia; yellow circles point to areas of coal dust particles. C, control group; L, low-dose coal dust group; M, medium-dose coal dust group; H, high-dose coal dust group. $n = 4$. Compared with the control group at the corresponding time points, $*P < 0.05$, $\#P < 0.01$. (For interpretation of the references to color in this figure legend, the reader is referred to the web version of this article.)

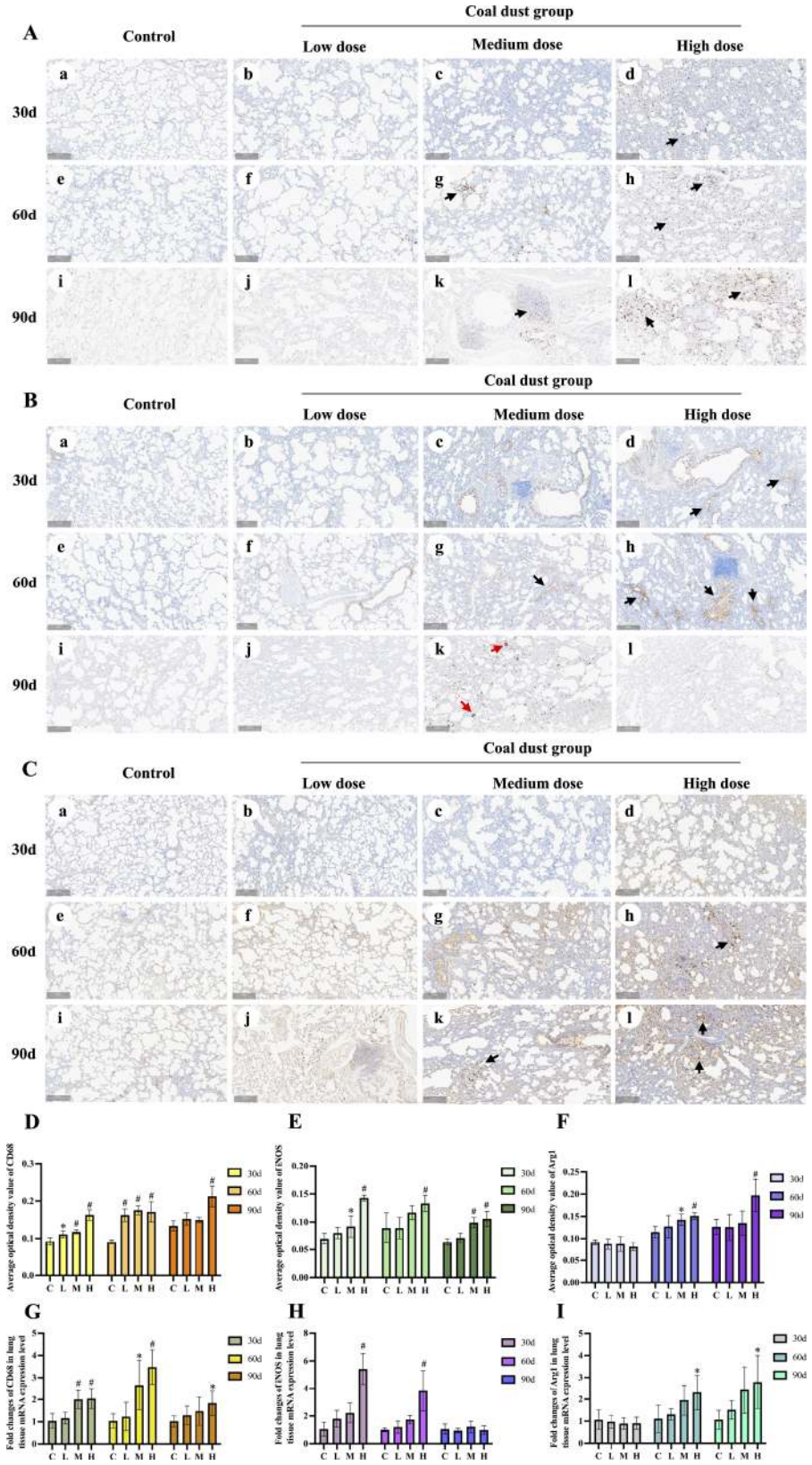

Fig. 5. Expression of various types of macrophages in rat lung tissue. A-C show the expression of the macrophage marker CD68, the M1 macrophage marker iNOS and the M2 macrophage marker Arg1 (10X). D-F are the results of quantitative analysis of different types of macrophages. G-I are the mRNA expression levels of various macrophage markers in rat lung tissue. The black arrow points to the area of positive expression; the red arrow points to the area of coal dust particles. C, control group; L, low-dose coal dust group; M, medium-dose coal dust group; H, high-dose coal dust group. $n = 4$. Compared with the control group at the corresponding time points, $*P < 0.05$, $\#P < 0.01$. (For interpretation of the references to color in this figure legend, the reader is referred to the web version of this article.)

3.6. Expression of M1 macrophage-associated cytokines

M1 macrophages could secrete inflammatory cytokine and chemokines to involve in the up-regulation of inflammatory reactions. The expression levels of M1 macrophage-associated inflammatory cytokines (IL-6, TNF-α, IL-1β) and chemokines (IL-8, CCL2, CCL5) in rat lung tissue after exposure were measured by RT-qPCR and ELISA (Fig. 6A-F). RT-qPCR results showed that all six cytokines peaked at day 60 of coal dust exposure and then decreased, with *CCL5* being 356.82 times higher in the high dose group than in the control group after 60 days of coal dust exposure, with the most significant trend. ELISA results showed that IL-6 in rat serum, lung tissue and BALF peaked and then decreased after 30 days of high-dose coal dust exposure (Fig. 6G-I). TNF-α in lung tissue and BALF peaked at 30 days of coal dust exposure, while TNF-α in serum peaked at 60 days (Fig. 6J-L). IL-1β in serum, lung tissue and BALF peaked at 60 days of coal dust exposure (Fig. 6M-O). The chemokines IL-8 (Fig. 6P-R), CCL2 (Fig. 6S-U) and CCL5 (Fig. 6V-X) in serum and lung tissues all peaked at 60 days of coal dust exposure, followed by a decreasing trend, similar to the RT-qPCR results. The ELISA results showed the most significant changes in the protein levels of CCL5 in BALF, with increases of 5.30-fold, 4.73-fold and 4.47-fold in the high dose group at various time points compared with the control group at the corresponding time points. These results indicated that M1 macrophages play a dominant role within the first 60 days of coal dust exposure.

3.7. Expression of M2 macrophage-related cytokines

M2 macrophages, also known as anti-inflammatory macrophages, could secrete IL-10, TGF-β and other factors involved in the anti-inflammatory and pro-fibrotic processes. RT-qPCR results showed that *IL-10* mRNA level in rat lung tissue increased with the duration and dose of coal dust exposure, peaking at 60 days of dust exposure with a 6.03-fold increase in the high dose group compared with the control group (Fig. 7A). *TGF-β* mRNA level in rat lung tissue were inversely correlated with dust dose after 30 days of coal dust exposure while positively correlated after 60 and 90 days. Compared with the control group at the corresponding time points, *TGF-β* mRNA levels were 5.56 and 6.17 times higher in the 60 and 90 days high dose groups, respectively (Fig. 7B), with a statistically significant difference ($P < 0.01$). The mRNA levels of *Gas6* showed a general trend of decrease (30 days), increase (60 days), and decrease (90 days) throughout the duration of coal dust exposure. Taking coal dust exposure for 60 days as an example, *Gas6* mRNA levels were 66.99-fold higher in the lung tissue in the high dose group compared with the control group (Fig. 7C). ELISA results showed similar trends for IL-10 and TGF-β in serum, lung tissue and BALF, all of which were significantly elevated at 60 days and persistently elevated at 90 days (Fig. 7D-I). The expression level of Gas6 showed a more complex trend - its expression in serum was proportional to the duration and dose of coal dust exposure, while showed a decreasing trend in BALF at 30 days and in lung tissue at 90 days (Fig. 7J-L).

Among the above indicators, the changes in serum TGF-β were the most significant, with increases of 3.92-fold, 5.65-fold and 12.43-fold in the high dose group at 30, 60, and 90 days compared with the control group.

4. Discussion

4.1. Simulation of exposure parameters of the real working environment of coal miners is an important consideration for establishing a rat model of coal worker pneumoconiosis in this study

The severity of CWP was directly related to the cumulative dust exposure and exposure time of coal miners [29]. On the basis of referring to the relevant occupational health standards for dust concentration limits in occupational places (see Materials and Methods section for details), in this study, a control group and three dose groups with low (4 mg/m^3), medium (10 mg/m^3) and high coal dust exposure were set up. Studies have shown that a year for humans is equivalent to nine days for rats [30], while it took about 5–10 years averagely for the coal miner to develop pneumoconiosis, so the total period of the experiment was 90 days, which was approximately equivalent to 10 years for humans.

For dynamic inhalation exposure, fresh air containing a certain concentration of test substance was sent into the cabinet through mechanical ventilation, and the same amount of polluted gas was discharged at the same time, so that the concentration of test substance in the cabinet can maintain dynamic equilibrium. The biggest advantage of dynamic inhalation exposure was that it could better simulate human exposure in the actual working environment, making the study results more realistic [31]. Compared with frequently used single endotracheal instillation, dynamic inhalation exposure did not cause artificial damage to the lungs, which could avoid the inflammatory response of the respiratory tract due to improper handling and reduce interference with subsequent measurement of inflammatory factors. Compared with static inhalation exposure, dynamic inhalation exposure could keep the concentration and oxygen partial pressure of the subject in a relatively stable state, which was more suitable for sub-chronic and chronic poisoning with low concentration and long duration.

In summary, the dynamic inhalation exposure, dose design, and duration of exposure used in this study were selected with reference to realistic exposure scenarios of coal miners. The results of the bibliometric analysis indicated that very few studies have been able to simultaneously simulate these three key exposure parameters based on real scenarios. Therefore, this was one of the main innovations of this study.

4.2. Coal dust exposure caused growth retardation, increased lung organ coefficients and reduced lung function in rats

Abnormal weight changes were considered to be a veritable indicator of toxicity [32]. In this study, compared with the control group, the rats in the coal dust exposure groups gained weight slowly. After 90 days of exposure, the rats in all the coal dust exposure groups showed a decreasing trend in body weight compared with the control group. This suggested that exposure to coal dust could cause decreased appetite in rats, and thus lead to delayed growth and development.

The organ coefficient is the ratio of organ weight to body weight. When inhalable dust is inhaled into the lungs, it causes an increase in inflammatory reactions in the lung tissue, manifested as infiltration of inflammatory cells and edema of the lung tissue, and ultimately leading to an increase in lung tissue weight. Similarly, in this study, the lung organ coefficient of rats exposed to dust increased compared to the control group at 60 and 90 days of exposure. This result suggested that coal dust exposure could lead to an increase in inflammatory reactions in rat lung tissue.

According to the previous research, patients with pneumoconiosis suffered from severe inflammatory cell infiltrations, resulting in decreased elastic retraction of the lungs, narrowed airways, and increased resistance of small airways, resulting in reduced pulmonary ventilation and decreased gas diffusion area, which eventually leads to gas exchange dysfunction between alveoli and capillaries [33–34]. Pulmonary function tests can be used to effectively assess airflow restriction. Commonly used pulmonary function tests include respiratory rate, tidal volume, vital capacity and inspiratory capacity, among others. Respiratory rate is the number of breaths per minute and can be used to observe the status of respiratory function. When the respiratory rate increases, it indicates tachypnea. Tidal volume is the volume of gas inhaled or exhaled each time during calm breathing, and is an indicator of lung volume, mainly used for pulmonary ventilation function tests. Low tidal volume values indicate inadequate lung ventilation, while high values indicate hyperventilation. The lower the tidal volume, the higher the respiratory rate is required to ensure adequate ventilation

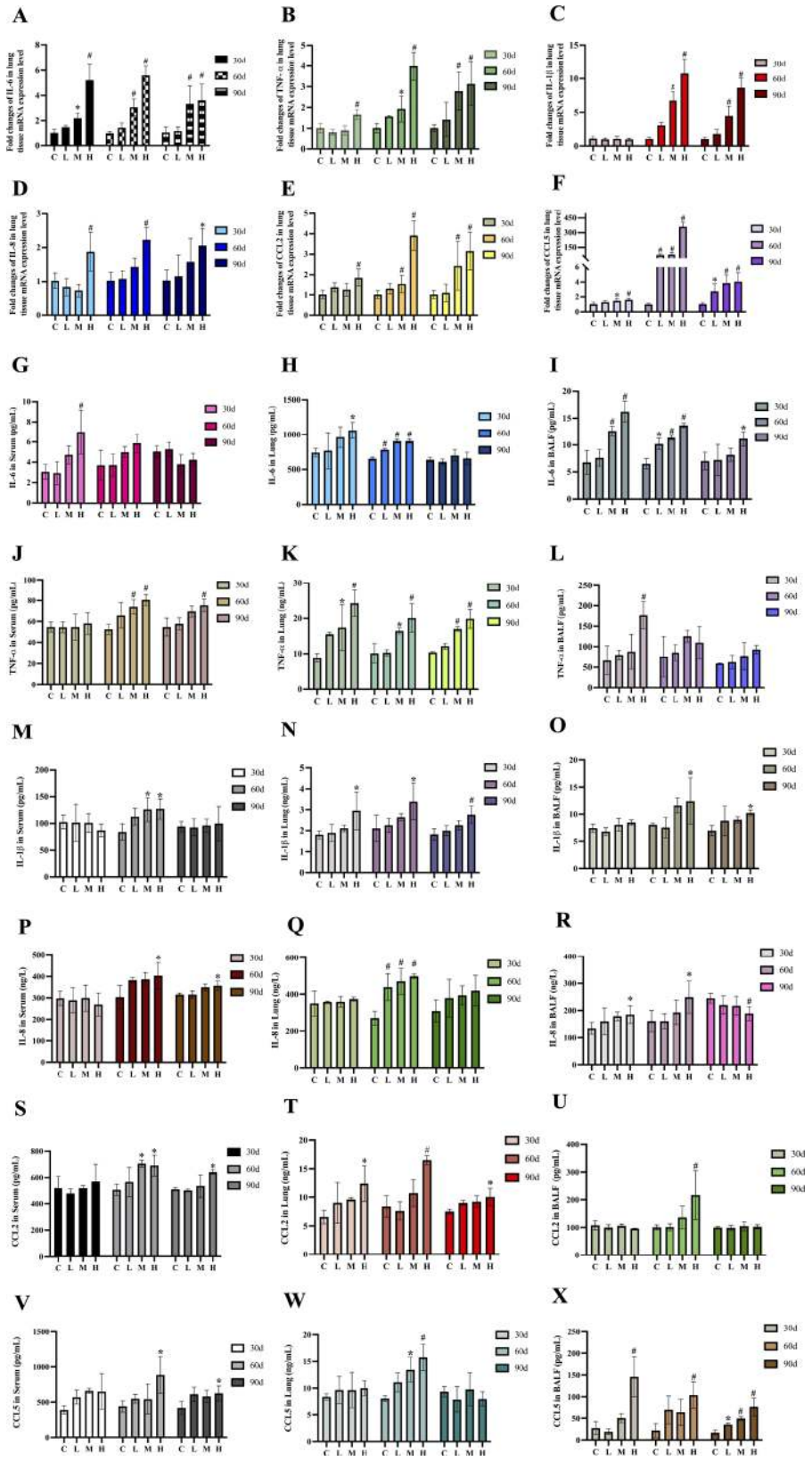

Fig. 6. Changes in mRNA and protein levels of cytokines associated with M1 macrophages in lung tissue. A-F are the mRNA expression levels of *IL-6, TNF-α, IL-1β, IL-8, CCL2* and *CCL5* in lung tissue. G-X are the protein levels of IL-6, TNF-α, IL-1β, IL-8, CCL2 and CCL5 in serum, lung tissue and BALF respectively. C, control group; L, low-dose coal dust group; M, medium-dose coal dust group; H, high-dose coal dust group. $n = 6$. Compared with the control group at the corresponding time points, $^{*}P < 0.05$, $\#P < 0.01$.

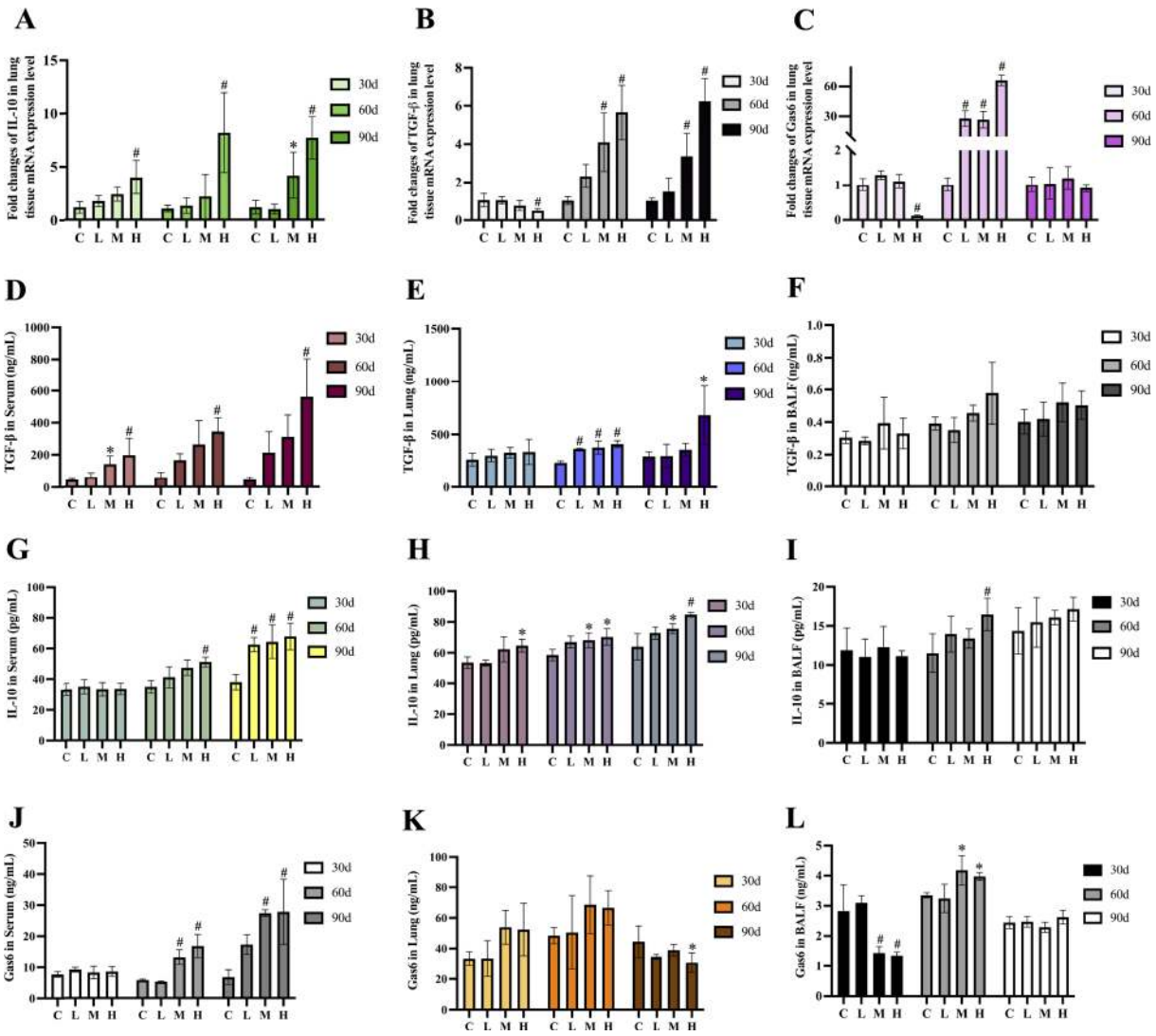

Fig. 7. Changes in mRNA and protein levels of cytokines associated with M2 macrophages in lung tissue. A-C for mRNA expression of IL-10, TGF-β, and Gas6 in lung tissue. D-L are protein levels of IL-10, TGF-β and Gas6 in serum, lung tissue and BALF respectively. C, control group; L, low-dose coal dust group; M, medium-dose coal dust group; H, high-dose coal dust group. $n = 6$. Compared with the control group at the corresponding time points, $^{*}P < 0.05$, $^{\#}P < 0.01$.

[35]. Restrictive lung diseases such as pulmonary fibrosis and pulmonary edema are usually characterized by shallow and rapid breathing with increased respiratory rate and decreased tidal volume [36–37].

Vital capacity refers to the volume of gas exhaled to the best of one's ability after maximum inspiration, and also belongs to the ventilation function index. When tidal volume and vital capacity decrease, it indicates pulmonary ventilation dysfunction. Inspiratory capacity is the amount of gas that can be inhaled when making maximum inspiration from the end of calm expiration and is an important indicator of maximum ventilation potential. In this study, the results of pulmonary function measurements indicated that coal dust exposure could increase the respiratory rate of rats, reduce tidal volume, vital capacity, and inspiratory capacity, suggesting that the ventilation function of rats was limited and their lung function was reduced.

4.3. Pulmonary macrophage polarization may play a very important role in the pathological process of CWP

The features of CWP mainly manifest as persistent inflammatory response and fibrotic lesions in the lungs. In this study, HE and Masson staining of paraffin sections revealed inflammatory and fibrotic lesions in the lungs of coal dust-exposed rats, and the degree of pathological changes were positively correlated with the dose and duration of coal dust exposure. Meanwhile, the mRNA expression levels of lung fibrosis-related proteins (*FN1, COL-1*) and mesenchymal cell marker (*α-SMA*) were all significantly increased, while the mRNA level of epithelial cell marker (*E-cad*) was significantly decreased on the 60th day of coal dust exposure.

Scholars have proposed various theories for the pathogenesis of CWP, but none of them can fully describe its pathological process. It is generally believed that lung macrophages can be activated during phagocytosis and clearance of coal dust, which induces persistent inflammation and abnormal tissue repair, and ultimately leading to pulmonary fibrosis [38]. As multi-functional intrinsic immune cells in lung tissue, lung macrophages not only activate the inflammatory response but also initiate fibrosis, demonstrating the critical role of macrophages in the tissue inflammatory response and fibrosis [39]. The specific function of macrophages could be directly influenced by the direction of macrophage polarization. It is generally accepted that an abnormal polarization of macrophages can lead to an inflammatory response and tissue fibrosis [40–41]. Studies have shown that macrophage polarization imbalances are present in various diseases [42–44]. Therefore, an in-depth investigation of the relationship between macrophage polarization and CWP may provide a scientific reference for

investigating the mechanism of CWP.

Alveolar macrophages are the first line of defense in the lungs [45]. When coal dust particles enter the lung tissue, lung macrophages recognize and engulf the coal dust particles, leading to the recruitment of more macrophages as more coal dust particles enter the lung tissue, resulting in an increase in the number of lung macrophages [38]. The results of this study showed that the macrophage marker CD68 in lung tissue tended to increase with the dose and duration of coal dust exposure, suggesting that exposure might cause aggregation of macrophages in lung tissue. Pulmonary macrophages were involved in the pathogenesis of many lung diseases by polarizing into two functionally opposite phenotypes (M1/M2) in response to microenvironmental signals [46]. The immunohistochemistry results showed that expression levels of the M1 macrophage marker iNOS in the lung tissue of rats exposed to coal dust at 30, 60, and 90 days showed an increasing trend with the increase of coal dust exposure dose. A comparison of iNOS expression in the coal dust exposure groups at the three-time points showed that iNOS expression peaked after 60 days of coal dust exposure and showed a decreasing trend after 90 days. Meanwhile, the expression levels of *iNOS* mRNA in the lung tissue also increased significantly after 30 days of the coal dust exposure. However, as the dust exposure time prolonged, the expression in the coal dust exposure group gradually returned to a level similar to that of the control group. These results suggested that macrophages could be activated by coal dust, causing an inflammatory response and that M1 macrophages played an important role in the early stage of CWP. Initially, the presence of these inflammatory mediators was beneficial, helping to stimulating adaptive immunity [47].

With the progress of inflammation, when the lung injury reached a certain degree, the pulmonary macrophages will polarize to M2 type to protect the body from inflammatory injury and trigger wound healing to start tissue repair [48–49]. The results of this study showed that the M2 macrophage marker *Arg1* began to increase after 60 days of coal dust exposure and reached its peak at 90 days. Immunohistochemical result was similar to the relative expression of *Arg1* mRNA in lung tissue. The above results were consistent with the reports in the relevant literature [10,20,50], which confirmed that the pathological process of CWP was closely related to the dynamic changes of macrophage polarization - the inflammation phase is polarized to M1, while the fibrosis phase was polarized to M2.

4.4. Effect of coal dust exposure on macrophage polarization-related cytokine expression levels - time, dose, and tissue specimen type specificity

In this experiment, the cytokines were tested in serum, lung tissue, and BALF, respectively, to provide a more comprehensive picture of cytokine changes in the different samples. M1 macrophages secreted IL-6, TNF-α, IL-1β, CCL2, IL-8, CCL5 and other proinflammatory cytokines [42]. IL-6 and IL-1β were members of the interleukin family, multipotent cytokines that send inflammatory signals from local lesions throughout the body and stimulate the recruitment of immune cells, including monocytes/macrophages [51]. TNF-α, a cytokine produced by a variety of cells including macrophages, natural killer cells, and T cells, was involved in local inflammation and could also induce the production of other cytokines and activate and promote the synthesis and secretion of other inflammatory factors [52]. In this study, IL-6 reached a peak at 30 days in serum, lung tissue, and BALF, suggesting that IL-6 may be a cytokine that responded earlier to coal dust stimulation [53]. While TNF-α peaked at 30 days in lung tissue and BALF, it peaked at 60 days in serum, suggesting an earlier response in lung tissue compared with serum. IL-1β peaked at 60 days in all three different types of samples, suggesting that IL-1β may respond later than IL-6 and TNF-α. When coal dust entered the body, it first irritated the lung tissue, which as a target organ could respond much earlier, with subsequent changes in cytokines in BALF and serum. Compared with BALF, the fold changed in cytokines in serum and lung tissue were more pronounced.

Chemokines were cytokines that recruit immune cells such as monocytes, lymphocytes, dendritic cells, and natural killer cells, and were responsible for regulating the type and number of immune cells in inflammatory response [54]. Chemokines were typically divided into three subfamilies - CXC, CC, and CX3C [55]. IL-8, also known as CXCL8, was a widely sourced cytokine belonging to the CXC subfamily with neutrophil chemotactic activity [56]. Research have shown that the levels of IL-8 in the serum, lung lavage fluid, or induced sputum of pneumoconiosis patients were significantly higher than those of workers in the control group [57–58]. Similarly, in this study, compared to the control group, the levels of IL-8 in rat serum and BALF were directly proportional to the exposure time and dose at 30 and 60 days. At 60 and 90 days of exposure, the content of IL-8 in the lung tissue of the coal dust exposed group increased. As the dust exposure time prolonged, the expression levels of CCL2 and CCL5 showed a trend of increasing (at 30 days), peaking (at 60 days), and decreasing (at 90 days), which was consistent with their mediating pro-inflammatory physiological functions and was also similar to the research results in the literature [59].

M2 macrophages mainly exerted anti-inflammatory and fibrogenic effects by secreting anti-inflammatory factors such as IL-10 and TGF-β [42]. Coincidentally, in this study, the mRNA and protein expression levels of IL-10 and TGF-β in lung tissue increased with the prolongation of dust exposure time, reaching peak values at 90 days. By comparing three different types of tissue specimens horizontally, it could be seen that compared with the control group, the expression levels of IL-10 and TGF-β in the lung tissue and serum of rats in the coal dust exposed group showed more significant changes in multiple factors.

5. Conclusion

In this study, with reference to the exposure parameters (exposure route, exposure dose and exposure duration) of coal miners in the real working environment, a rat model of CWP was established. The results showed that macrophage polarization played an important role in the pathological process of CWP, which was mainly manifested in M1 polarization in the inflammatory phase and M2 polarization in the fibrosis phase. It was worth noting that among the nine cytokines measured, the expression level of *CCL5* mRNA showed the most significant multiple changes, much greater than TNF-α (the earliest and most important pro-inflammatory factor that appeared during the inflammatory response), suggesting that this chemokine plays an important role in the progression of CWP and warrants further investigation.

Funding

This study was supported by Key Research and Development Program of Ningxia Hui Autonomous Region [grant number: 2021BEG02030], Ningxia Natural Science Foundation [grant number: 2022AAC05027], and National Natural Science Foundation of China [grant number: 81660527].

CRediT authorship contribution statement

Rui Wang: Conceptualization, Formal analysis, Writing – original draft, Writing – review & editing. **Siyi Zhang:** Conceptualization, Writing – original draft, Writing – review & editing. **Yifei Liu:** Conceptualization, Formal analysis. **Hongmei Li:** Conceptualization, Writing – review & editing. **Suzhen Guan:** Conceptualization, Writing – review & editing. **Lingqin Zhu:** Formal analysis. **Leina Jia:** Formal analysis. **Zhihong Liu:** Conceptualization, Formal analysis, Writing – original draft, Writing – review & editing. **Haiming Xu:** Conceptualization, Formal analysis, Writing – original draft, Writing – review & editing.

Declaration of Competing Interest

The authors declare that they have no known competing financial interests or personal relationships that could have appeared to influence the work reported in this paper.

Data availability

The authors do not have permission to share data.

References

[1] T. Liu, S. Liu, The impacts of coal dust on miners' health: A review, Environ. Res. 190 (2020), 109849.
[2] W. Liu, R. Liang, R. Zhang, et al., Prevalence of coal worker's pneumoconiosis: a systematic review and meta-analysis, Environ. Sci. Pollut. Res. Int. 29 (59) (2022) 88690–88698.
[3] Y. Song, K. Southam, B.B. Beamish, et al., Effects of chemical composition on the lung cell response to coal particles: Implications for coal workers' pneumoconiosis, Respirology 27 (6) (2022) 447–454.
[4] J.A. Gimenes Jr, V. Srivastava, H. ReddyVari, et al., Rhinovirus-induces progression of lung disease in a mouse model of COPD via IL-33/ST2 signaling axis, Clin. Sci. (Lond.) 133 (8) (2019) 983–996.
[5] L. Wang, Y. Zhang, N. Zhang, et al., Potential role of M2 macrophage polarization in ventilator-induced lung fibrosis, Int. Immunopharmacol. 75 (2019), 105795.
[6] M. Yang, X. Qian, N. Wang, et al., Inhibition of MARCO ameliorates silica-induced pulmonary fibrosis by regulating epithelial-mesenchymal transition, Toxicol. Lett. 301 (2019) 64–72.
[7] X. Liu, S. Fang, H. Liu, et al., Role of human pulmonary fibroblast-derived MCP-1 in cell activation and migration in experimental silicosis, Toxicol. Appl. Pharmacol. 288 (2) (2015) 152–160.
[8] J.M. Mayeux, G.M. Escalante, J.M. Christy, et al., Silicosis and Silica-Induced Autoimmunity in the Diversity Outbred Mouse, Front. Immunol. 9 (2018) 874.
[9] C.D. Richards, Innate Immune Cytokines, Fibroblast Phenotypes, and Regulation of Extracellular Matrix in Lung, J. Interferon Cytokine Res. 37 (2) (2017) 52–61.
[10] Y. Zhao, C. Hao, L. Bao, et al., Silica particles disorganize the polarization of pulmonary macrophages in mice, Ecotoxicol. Environ. Saf. 193 (2020), 110364.
[11] P.J. Murray, Macrophage Polarization, Annu. Rev. Physiol. 79 (2017) 541–566.
[12] N.R. Aggarwal, L.S. King, F.R. D'Alessio, Diverse macrophage populations mediate acute lung inflammation and resolution, Am. J. Physiol. Lung Cell. Mol. Physiol. 306 (8) (2014) L709–L725.
[13] C. Yunna, H. Mengru, W. Lei, et al., Macrophage M1/M2 polarization, Eur. J. Pharmacol. 877 (2020), 173090.
[14] T.C. Huang, H.L. Wu, S.H. Chen, et al., Thrombomodulin facilitates peripheral nerve regeneration through regulating M1/M2 switching, J. Neuroinflammation 17 (1) (2020) 240.
[15] A. Shapouri-Moghaddam, S. Mohammadian, H. Vazini, et al., Macrophage plasticity, polarization, and function in health and disease, J. Cell. Physiol. 233 (9) (2018) 6425–6440.
[16] Y. Tong, Z. Yu, Z. Chen, et al., The HIV protease inhibitor saquinavir attenuates sepsis-induced acute lung injury and promotes M2 macrophage polarization via targeting matrix metalloproteinase-9, Cell Death Dis. 12 (1) (2021) 67.
[17] T. Xiao, Z. Zou, J. Xue, et al., LncRNA H19-mediated M2 polarization of macrophages promotes myofibroblast differentiation in pulmonary fibrosis induced by arsenic exposure, Environ. Pollut. 268 (Pt A) (2021), 115810.
[18] R. Uchiyama, E. Toyoda, M. Maehara, et al., Effect of platelet-rich plasma on M1/M2 macrophage polarization, Int. J. Mol. Sci. 22 (5) (2021) 2336.
[19] J. Liu, Z. Zhang, Y. Yang, et al., NCOA4-Mediated ferroptosis in bronchial epithelial cells promotes macrophage M2 polarization in COPD emphysema, Int. J. Chron. Obstruct. Pulmon. Dis. 17 (2022) 667–681.
[20] Q. Tang, C. Xing, M. Li, et al., Pirfenidone ameliorates pulmonary inflammation and fibrosis in a rat silicosis model by inhibiting macrophage polarization and JAK2/STAT3 signaling pathways, Ecotoxicol. Environ. Saf. 244 (2022), 114066.
[21] S. Li, S. Gao, Q. Jiang, et al., Clevudine attenuates bleomycin-induced early pulmonary fibrosis via regulating M2 macrophage polarization, Int. Immunopharmacol. 101 (Pt B) (2021), 108271.
[22] S.L. Zhao, M.M. Liu, H. Li, et al., Comparison between pyrophosphate method and infrared spectrophotometry for determination of silicon dioxide content in dust, Zhonghua Lao Dong Wei Sheng Zhi Ye Bing Za Zhi 37 (10) (2019) 781–784.
[23] K.B. Beć, J. Grabska, C.W. Huck, Near-Infrared Spectroscopy in Bio-Applications, Molecules 25 (12) (2020) 2948.
[24] M. Germine, J.H. Puffer, Analytical transmission electron microscopy of amosite asbestos from South Africa, Arch. Environ. Occup. Health 75 (1) (2020) 36–44.
[25] M. Alkholief, M.A. Kalam, A.K. Alshememry, et al., Topical Application of Linezolid-Loaded Chitosan Nanoparticles for the Treatment of Eye Infections, Nanomaterials (Basel). 13 (4) (2023) 681.
[26] S.V. Szapiel, N.A. Elson, J.D. Fulmer, et al., Bleomycin-induced interstitial pulmonary disease in the nude, athymic mouse, Am. Rev. Respir. Dis. 120 (4) (1979) 893–899.
[27] F. Dai, Q. Zhuang, G. Huang, et al., Infrared Spectrum Characteristics and Quantification of OH Groups in Coal, ACS Omega 8 (19) (2023) 17064–17076.
[28] M.M. Mabrouk Zayed, H.A. Sahyon, N.A.N. Hanafy, et al., The Effect of Encapsulated Apigenin Nanoparticles on HePG-2 Cells through Regulation of P53, Pharmaceutics. 14 (6) (2022) 1160.
[29] N.B. Hall, D.J. Blackley, C.N. Halldin, et al., Current Review of Pneumoconiosis Among US Coal Miners, Curr. Environ. Health Rep. 6 (3) (2019) 137–147.
[30] S. Dutta, P. Sengupta, Men and mice: Relating their ages, Life Sci. 152 (2016) 244–248.
[31] Y. Zhang, C. Long, G. Hu, et al., Two-week repair alleviates hexavalent chromium-induced hepatotoxicity, hepatic metabolic and gut microbial changes: A dynamic inhalation exposure model in male mice, Sci. Total Environ. 857 (Pt 1) (2023), 159429.
[32] S. Teo, D. Stirling, S. Thomas, et al., A 90-day oral gavage toxicity study of D-methylphenidate and D,L-methylphenidate in Sprague-Dawley rats, Toxicology. 179 (3) (2002) 183–196.
[33] Y. Fan, R. Ma, X. Du, et al., Small airway dysfunction in pneumoconiosis: a cross-sectional study, BMC Pulm. Med. 22 (1) (2022) 167.
[34] E.L. Petsonk, R.C. Stansbury, L.A. Beeckman-Wagner, et al., Small Airway Dysfunction and Abnormal Exercise Responses. A Study in Coal Miners, Ann. Am. Thorac. Soc. 13 (7) (2016) 1076–1080.
[35] M.S. Jo, B.W. Kim, Y.H. Kim, et al., The Acute and Short-Term Inhalation of Carbon Nanofiber in Sprague-Dawley Rats, Biomolecules 12 (10) (2022) 1351.
[36] J.H. Sung, B.G. Choi, S.H. Maeng, et al., Recovery from welding-fume-exposure-induced lung fibrosis and pulmonary function changes in sprague dawley rats, Toxicol. Sci. 82 (2) (2004) 608–613.
[37] P. Sharma, J. Alizadeh, M. Juarez, et al., Autophagy, Apoptosis, the Unfolded Protein Response, and Lung Function in Idiopathic Pulmonary Fibrosis, Cells. 10 (7) (2021) 1642.
[38] M. Mu, B. Li, Y. Zou, et al., Coal dust exposure triggers heterogeneity of transcriptional profiles in mouse pneumoconiosis and Vitamin D remedies, Part. Fibre Toxicol. 19 (1) (2022) 7.
[39] M. Mack, Inflammation and fibrosis, Matrix Biol. 68–69 (2018) 106–121.
[40] E.M. Kim, Y.S. Kwak, M.H. Yi, et al., Clonorchis sinensis antigens alter hepatic macrophage polarization in vitro and in vivo, PLoS Negl. Trop. Dis. 11 (5) (2017) e0005614.
[41] V. Le, E.D. Crouser, Potential immunotherapies for sarcoidosis, Expert Opin. Biol. Ther. 18 (4) (2018) 399–407.
[42] C. Wang, C. Ma, L. Gong, et al., Macrophage polarization and its role in liver disease[J], Front. Immunol. 12 (2021), 803037.
[43] S. Eshghjoo, D.M. Kim, A. Jayaraman, et al., Macrophage Polarization in Atherosclerosis, Genes (Basel) 13 (5) (2022) 756.
[44] A.J. Boutilier, S.F. Elsawa, Macrophage Polarization States in the Tumor Microenvironment, Int. J. Mol. Sci. 22 (13) (2021) 6995.
[45] R.F. Hamilton Jr, S.A. Thakur, A. Holian, Silica binding and toxicity in alveolar macrophages, Free Radic. Biol. Med. 44 (7) (2008) 1246–1258.
[46] A.C. McQuattie-Pimentel, G.R.S. Budinger, M.N. Ballinger, Monocyte-derived Alveolar Macrophages: The Dark Side of Lung Repair? Am. J. Respir. Cell Mol. Biol. 58 (1) (2018) 5–6.
[47] C. Nathan, A. Ding, Nonresolving inflammation, Cell 140 (6) (2010) 871–882.
[48] X. Hu, H. Wang, C. Han, et al., Src promotes anti-inflammatory (M2) macrophage generation via the IL-4/STAT6 pathway, Cytokine 111 (2018) 209–215.
[49] B. Galliot, M. Crescenzi, A. Jacinto, et al., Trends in tissue repair and regeneration, Development 144 (3) (2017) 357–364.
[50] Z. Zhang, X. Wu, G. Han, et al., Altered M1/M2 polarization of alveolar macrophages is involved in the pathological responses of acute silicosis in rats in vivo, Toxicol. Ind. Health 38 (12) (2022) 810–818.
[51] T. Tanaka, M. Narazaki, T. Kishimoto, Immunotherapeutic implications of IL-6 blockade for cytokine storm, Immunotherapy 8 (2016) 959–970.
[52] I. Ates, B. Yucesoy, A. Yucel, et al., Possible effect of gene polymorphisms on the release of TNFα and IL1 cytokines in coal workers' pneumoconiosis, Exp. Toxicol. Pathol. 63 (1–2) (2011) 175–179.
[53] T. Tanaka, M. Narazaki, T. Kishimoto, IL-6 in inflammation, immunity, and disease, Cold Spring Harb. Perspect. Biol. 6 (10) (2014), a016295.
[54] J. Lee, I. Arisi, E. Puxeddu, et al., Bronchoalveolar lavage (BAL) cells in idiopathic pulmonary fibrosis express a complex pro-inflammatory, pro-repair, angiogenic activation pattern, likely associated with macrophage iron accumulation, PLoS One 13 (4) (2018) e0194803.
[55] A. Zlotnik, O. Yoshie, Chemokines: a new classification system and their role in immunity, Immunity 12 (2) (2000) 121–127.
[56] G. Lecio, F.V. Ribeiro, S.P. Pimentel, et al., Novel 20% doxycycline-loaded PLGA nanospheres as adjunctive therapy in chronic periodontitis in type-2 diabetics: randomized clinical, immune and microbiological trial, Clin. Oral Invest. 24 (3) (2020) 1269–1279.
[57] M. Gulumian, P.J. Borm, V. Vallyathan, et al., Mechanistically identified suitable biomarkers of exposure, effect, and susceptibility for silicosis and coal-worker's pneumoconiosis: a comprehensive review, J. Toxicol. Environ. Health B Crit. Rev. 9 (5) (2006) 357–395.
[58] J.S. Lee, J.H. Shin, B.S. Choi, Serum levels of IL-8 and ICAM-1 as biomarkers for progressive massive fibrosis in coal workers' pneumoconiosis, J. Korean Med. Sci. 30 (2) (2015) 140–144.
[59] R. Nadif, M. Mintz, S. Rivas-Fuentes, et al., Polymorphisms in chemokine and chemokine receptor genes and the development of coal workers' pneumoconiosis, Cytokine 33 (3) (2006) 171–178.